ADVANCED HEALTHCARE MATERIALS
www.advhealthmat.de

Extracellular Matrix-Mediated Crosslinking of Adhesive Hyaluronic Acid Patch for Treating Volumetric Muscle Injury

Eun Je Jeon, Soohwan An, Seung Yeop Han, Eunseon Jeong, Young Seok Song, Jung Seung Lee, and Seung-Woo Cho**

The treatment of volumetric muscle loss (VML) is challenging owing to the deficiency of appropriate bioscaffolds and ineffective therapeutic outcomes with conventional approaches. Adhesive hydrogels have emerged as potential tools for promoting tissue regeneration, offering effective integration with damaged tissues. However, technical procedures requiring non-biocompatible crosslinking methods, mechanical mismatches, or the absence of tissue-specific microenvironments in conventional adhesive hydrogels have hindered their successful application in tissue reconstruction. In this study, a patch-type adhesive hydrogel is developed by combining a muscle tissue-derived extracellular matrix (MEM) and catechol-conjugated hyaluronic acid (HA-CA). This MEM-containing HA-CA (HCM) patch hydrogel utilizes MEM as both a biocompatible crosslinker and a therapeutic substance. The HCM patch hydrogel, crosslinked through a combination of covalent and non-covalent interactions via MEM and catechol in the composite, not only provides stable physical support but also develops muscle tissue-specific biochemical cues, mediating the recruitment and maturation of muscular cells. In animal models of VML, the HCM patch hydrogel effectively stimulates satellite cells and supports *de novo* muscle regeneration with functional restoration. This study emphasizes the efficacy and ready-to-use convenience of HCM patch hydrogels for muscle regeneration.

1. Introduction

Volumetric muscle loss (VML) caused by trauma or surgical ablation poses significant clinical challenges with limited therapeutic options, leading to functional deficits, disability, and compromised quality of life. Currently, VML treatments focus predominantly on using advanced braces or enhancing the strength of the existing muscle tissue, which usually provides limited functional restoration.[1] Alternatively, a muscle transposition or tendon transfer from an uninjured site can replace the defect, but their success rates are generally low.[2] In addition, these invasive procedures frequently confront significant morbidity at the donor site and side effects caused by inflammation, ineffective tissue integration, and reinnervation, which markedly reduce clinical outcomes.[3] Stem cell or muscle cell transplantation has been recognized as an innovative therapeutic strategy for various muscular diseases based on their regenerative capacity. However, transplanted cells usually encounter direct attack from the immune system and exhibit low engraft efficiency and long-term functionality, especially when these are transplanted into large cavities in the VML.[4,5] Although bioscaffolds have been evaluated for muscle regeneration, further research is required to optimize their efficacy and overcome the current limitations for successful muscle regeneration in VML.

Catechol-conjugated hyaluronic acid (HA-CA) hydrogels inspired by the underwater adhesion of marine organisms have been utilized for various tissue regenerations.[6–12] The tissue adhesive property of the HA-CA hydrogel by catechol chemistry can mediate a stable integration of the hydrogel construct, resulting

E. J. Jeon, S. An, S. Y. Han, E. Jeong, Y. S. Song, S.-W. Cho
Department of Biotechnology
Yonsei University
Seoul 03722, Republic of Korea
E-mail: seungwoocho@yonsei.ac.kr
E. J. Jeon, S.-W. Cho
Cellartgen Inc.
Seoul 03722, Republic of Korea
The ORCID identification number(s) for the author(s) of this article can be found under https://doi.org/10.1002/adhm.202403747

DOI: 10.1002/adhm.202403747

J. S. Lee
Department of Biomedical Engineering
Sungkyunkwan University
Suwon 16419, Republic of Korea
E-mail: jungseunglee@skku.edu
J. S. Lee
Department of Intelligent Precision Healthcare Convergence
Sungkyunkwan University
Suwon 16419, Republic of Korea
J. S. Lee
Department of MetaBioHealth
Sungkyunkwan University
Suwon 16419, Republic of Korea
S.-W. Cho
Center for Nanomedicine
Institute for Basic Science (IBS)
Seoul 03722, Republic of Korea

in improved cellular engraftment and functional maintenance at the injured site.[7,12–16] In general, catechol-functionalized polymers can be crosslinked mainly via oxidative covalent crosslinking and a combination of non-covalent interactions (e.g., electrostatic interactions, hydrophobic interactions, and hydrogen bonding) with the catechol moiety.[7,12] Although covalent bonding through catechol autoxidation occurs spontaneously, the reaction is very slow under physiological pH conditions and is insufficient to form a stable hydrogel without the addition of oxidants or enzymes with hydrogen peroxide (H_2O_2), which can potentially affect biocompatibility.[17] In addition, the technical difficulties in handling and preparing an optimal hydrogel construct based on the oxidation-dependent gelation process have constrained the successful translation of HA-CA hydrogels to the clinic.[17] To overcome these issues, a patch-type HA-CA was developed earlier as a ready-to-use format for efficient cell transplantation and drug delivery. However, it continues to rely on additives to enhance oxidation to form a robust gel construct.[14] Although HA-CA hydrogels support tissue regeneration by providing the adhesive and structural properties that facilitate cellular integration, these are deficient in the inherent biological activity required to directly activate the regenerative capacity of endogenous cells or promote their maturation for the successful recovery of injured muscle tissue.

In this study, we developed an HA-CA patch with enhanced reparative properties for the regeneration of volumetric muscle injury. A muscle tissue-derived extracellular matrix (MEM) was incorporated into the HA-CA hydrogel formulation (HCM) for enhanced tissue recovery by recruiting and activating endogenous muscle cells. Decellularization, a strategy for removing cellular components from native tissues, has been used extensively to prepare various types of scaffolds for tissue engineering owing to its remarkable regenerative properties and low immunogenicity.[18,19] MEM acquired from decellularization contains muscle tissue-specific biofunctional molecules that can provide muscle tissue-mimicking biochemical microenvironments and enhance muscle cell differentiation and maturation, in turn inducing enhanced regeneration.[19–21] Moreover, MEM facilitates the oxidation of HA-CA without the need for conventional oxidants by leveraging the enzymatic activities and hydrophobic interactions between the catechol groups and MEM proteins. We characterized the physicochemical properties of the HCM hydrogel and evaluated its capability to enhance muscle cell differentiation. Finally, the optimized HCM patch was applied to a VML mouse model to assess its therapeutic efficacy. This study highlights the potential of the HCM patch hydrogel as a ready-to-use product for muscle regeneration, suggesting its broad applicability in translational biomedicine.

2. Results and Discussion

2.1. Preparation and Characterization of HCM Patch Hydrogel

MEM was prepared from porcine muscle tissue via two decellularization steps using detergent solutions (Figure S1a, Supporting Information). After decellularization, the cell nuclei were removed successfully, while the extracellular matrix (ECM) components were preserved in the construct, which was verified by histological analyses using hematoxylin and eosin (H&E) and Masson's trichrome (MT) staining (**Figure 1**a). Quantitative analyses further demonstrated that the DNA content after decellularization decreased to less than 2% of that before decellularization, whereas the content of glycosaminoglycan (GAG) was retained at a level similar to that of the native tissue (Figure S1b, Supporting Information). These results demonstrate that MEM prepared through decellularization exhibits negligible immunogenicity but provides muscle tissue-specific biofunctional molecules. MEM was then solubilized and mixed with HA-CA, followed by lyophilization to prepare a patch-type HCM mixture (Figure 1a).

The gelation of the HCM patch can be initiated by adding a small volume of phosphate-buffered saline (PBS), which induces spontaneous networking between the MEM components and catechol moieties in HCM. After incubation at 37 °C for ≈10 min, the HCM patch transformed into hydrogel, displaying adhesive and cohesive properties. Meanwhile, the HA-CA patch without a MEM supplement remained as a solution under an identical condition and did not form a hydrogel (Figure S2, Supporting Information), suggesting a MEM-mediated crosslinking of HCM patch hydrogel. An inspection of the internal structure of the resulting hydrogel using scanning electron microscopy (SEM) verified that the MEM components were embedded within the HCM patch hydrogel (Figure 1b), consistent with a previous finding that demonstrated a similar ECM distribution within the ECM composite scaffold.[22] Although MEM plays a crucial role in the gelation of the HCM patch, the internal structure of the HCM patch hydrogel resembled that of the HA-CA patch hydrogel crosslinked by a conventional method using an oxidant (sodium periodate; $NaIO_4$), which is represented by interconnected micro-sized pores (HA-CA_ox; 102.4 ± 6.2 μm, HCM; 116.7 ± 17.0 μm) (Figure 1c). An SEM analysis was performed to reveal the similar internal structures of the two hydrogels, which demonstrated a similar gelation process for the HA-CA patch crosslinked by the oxidant and the HCM patch crosslinked by MEM.

2.2. Mechanical and Physical Properties of HCM Patch Hydrogels

The composition of the HCM patch hydrogel is primarily based on MEM and HA-CA, with MEM providing bioactive components that support muscle regeneration,[23,24] and HA-CA contributing to the structural stability. HA-CA_ox has also been studied for its potential use in muscle tissue regeneration.[15,25] The mechanical, adhesive, swelling, and degradation properties of the HA-CA_ox hydrogels have already been well-characterized in our previous studies.[14,26]

To prepare an adhesive and physically stable hydrogel system, we assessed the mechanical properties of the HCM patch hydrogel by adjusting the amount of MEM incorporated in the HCM patch. First, the rheological properties of the HCM patch hydrogels were investigated and compared with those of the control, HA-CA, and MEM hydrogels crosslinked using the conventional thermal incubation method (MEM).[23] In a frequency sweep mode, all the HCM patch hydrogels showed stable solid status, which was demonstrated by the elastic modulus (G') being continuously higher than the viscous modulus (G'') (Figure 1d; Figure S3, Supporting Information). The conventional MEM

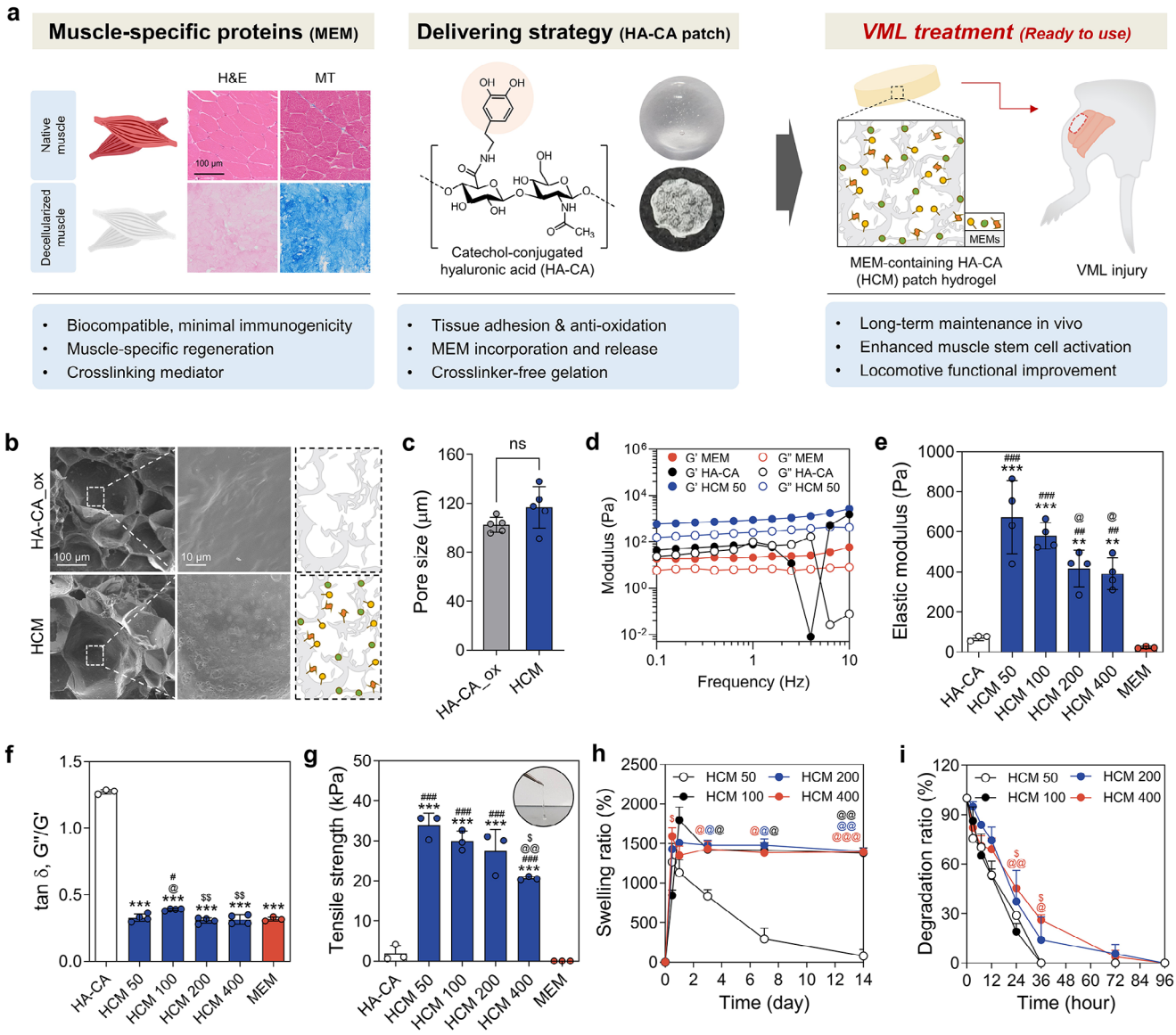

Figure 1. Characterization of muscle-derived extracellular matrix (MEM)-contained catechol-conjugated hyaluronic acid (HA-CA) (HCM) patch hydrogel. a) Schematic illustration describing the roles and advantages of two components (MEM and HA-CA patch) and the application of the MEM-containing HA-CA (HCM) patch hydrogel for VML treatment. b) Scanning electron microscopy (SEM) images of the cross-section of HA-CA patch hydrogel crosslinked by a $NaIO_4$ oxidant (HA-CA_ox) and a HCM patch hydrogel. c) Pore size analysis using SEM images ($n = 5$). d) Rheological analysis of hydrogel in a frequency sweep mode. The representative storage modulus (G′) and loss modulus (G″) were measured at a frequency range from 0.1 to 10 Hz. The HA-CA group indicates the HA-CA patch treated with phosphate-buffered saline (PBS). e) Average elastic modulus (G′) and f) elasticity (tan δ, G″ / G′) of the hydrogel at 1 Hz ($n = 3$–4). g) The tensile strength of hydrogel with different concentrations of MEM increased from 50 μg/mL to 400 μg/mL (HCM 50, 100, 200, and 400) ($n = 3$). h) Swelling property in PBS at 37 °C ($n = 5$), and i) degradation profile of hydrogel with 2.5 U/mL hyaluronidase ($n = 3$–5). The statistical difference was assessed using a two-sided *t*-test or one-way analysis of variance (ANOVA). The results are shown as mean ± S.D. (**$p < 0.01$ and ***$p < 0.001$ vs HA-CA; $^{\#}p < 0.05$, $^{\#\#}p < 0.01$, and $^{\#\#\#}p < 0.001$ vs MEM; $^{@}p < 0.05$, $^{@@}p < 0.01$, and $^{@@@}p < 0.001$ vs HCM 50; and $^{\$}p < 0.05$ and $^{\$\$}p < 0.01$ vs HCM 100).

hydrogel also formed a stable hydrogel. However, it showed a significantly lower elastic modulus than the HCM hydrogels (Figure 1d,e). Importantly, when the HA-CA patch without MEM was cross-linked spontaneously with PBS, the constructs were unstable, suggesting the importance of MEM in HCM patch hydrogel formation (Figure 1d). The elastic modulus of HCM hydrogels decreased gradually as the concentration of MEM increased from 50 to 400 μg mL^{-1} (HCM 50, 100, 200, and 400) (Figure 1e). It is noteworthy that the elasticity (tan δ) of the HCM hydrogels was similar to that of the MEM hydrogel regardless of the MEM concentration in the HCM hydrogel (Figure 1f). In contrast, the tan δ value of a MEM-free HA-CA patch treated with PBS was higher than one, indicating that its loss modulus was higher than the storage modulus. These results support the fact that HA-CA is difficult to self-crosslink without crosslinking agents such as MEM.

We also investigated the physical properties of the hydrogels in terms of their adhesiveness, swelling, and degradability. Over the past decade, catechol chemistry has been widely used to prepare adhesive hydrogels for various biomedical applications.[10,11] The adhesive property of catechol-modified hydrogels plays a crucial role in maintaining long-term performance and therapeutic efficacy through stable adhesion at the target site after transplantation.[7,13,16] The adhesion strength of the HCM hydrogel decreased as the amount of incorporated MEM increased (Figure 1g), which was probably attributed to the reduced interfacial accessibility of the catechol groups by the addition of MEM. However, considering that the MEM hydrogel has no adhesiveness, the adhesive properties of the HCM hydrogel are likely to contribute to its stable attachment to the desired site, potentially enhancing its practicability and therapeutic efficacy. The HA-CA patch hydrogel crosslinked with 200 μg mL^{-1} of MEM (HCM 200) developed in this study demonstrated a tensile adhesion strength of ≈27.5 kPa (Figure 1g), which is higher than that of various commercial tissue adhesives reported in the literature (≈20 kPa),[27,28] thus indicating its clinical potential.

Next, the swelling property of HCM hydrogel was tested by immersing the hydrogel constructs in PBS at 37 °C. The HCM hydrogels swelled rapidly within a day, particularly when these were crosslinked with 100, 200, and 400 μg mL^{-1} of MEM (Figure 1h). However, the swelling ratio of the HCM 50 patch hydrogels decreased gradually in PBS for 2 weeks (Figure 1h). This is because 50 μg mL^{-1} of MEM could generate a stable adhesive hydrogel, although insufficient to induce robust crosslinking for maintaining its shape and the networks in underwater conditions. For the in vitro degradation tests (Figure 1i), the HCM hydrogels were placed in a buffer solution containing hyaluronidase to replicate the in vivo environment. However, to rapidly compare the effects of MEM on the degradation rate of the hydrogels, the concentration of hyaluronidase was set at 2.5 U mL^{-1}, which is much higher than the typical hyaluronidase level observed in vivo (≈5.1 U L^{-1} in human serum).[29] The addition of 200 and 400 μg mL^{-1} MEM (HCM 200 and HCM 400 groups) increased crosslinking of HA-CA, which enhanced the network structure of the hydrogel, providing greater stability and resistance to degradation. On the other hand, the HCM 50 group exhibited the fastest degradation because MEM-induced crosslinking was the weakest among the tested groups. As shown in Figure 1h, HCM 50 hydrogel degraded rapidly, even in buffer conditions without hyaluronidase, due to the lower degree of crosslinking and structural integrity. In contrast, when the HCM 200 hydrogels were incubated in a buffer solution without hyaluronidase, the constructs did not degrade significantly for up to 2 weeks (Figure 1h). Although an increased amount of MEM lowered the elastic modulus and adhesion force of the HCM patch hydrogels, it is noteworthy that MEM participated in the crosslinking of the hydrogels and increased the robustness and stability of the construct, leading to delayed degradation.

For the mechanism study of the hydrogel formation, the HCM 200 group was selected as a representative group for the HCM patch hydrogel, considering its mechanical properties. HCM 50 and HCM 100 groups were excluded due to their lack of structural stability, as evidenced by the results of the swelling and degradation tests (Figure 1h,i). Although the mechanical properties of HCM 400 were comparable to those of HCM 200, it failed to provide optimized adhesiveness compared to the HCM 200 group (Figure 1g). As a result, HCM 200 was considered a representative group exhibiting stable mechanical properties with adhesiveness.

2.3. MEM-Mediated Crosslinking Mechanism of HCM Patch Hydrogel

Spectroscopic analyses were conducted to further investigate the effects of MEM on hydrogel formation. Free-radical oxidation is essential for the crosslinking process in catechol-based hydrogels because it facilitates the formation of covalent and non-covalent bonds critical for gelation.[12,30] As redox reactions drive the oxidative crosslinking of catechol-functionalized hydrogels, we first examined the hydroxyl radical scavenging activities of the materials. Both catechol, a known antioxidant,[31] and MEM, which contains various antioxidants such as myoglobin and peroxidase components,[32] play key roles in this process. When each substance was incubated with H_2O_2, HA-CA, HCM 200, and MEM exhibited considerable radical-scavenging activity compared with ascorbic acid (**Figure 2**a). It is noteworthy that MEM displayed the highest radical scavenging activity, and the activity of HCM 200, which consisted of both HA-CA and MEM, was lower than that of MEM alone (Figure 2a). It is likely that the peroxidase activity of MEM might be consumed to oxidize catechol in HA-CA during autoxidation, thereby causing a decrease in the overall radical scavenging activity of MEM in HCM.

Considering these oxidative properties, MEM was considered to facilitate oxidative crosslinking of HA-CA. Catechol can be auto-oxidized to the semiquinone radical and quinone with oxygen to form O_2^- and H_2O_2.[33] However, under physiological conditions, the reaction does not occur sufficiently to induce the oxidative crosslinking of catechol-functionalized polymers actively. However, the peroxidase included in the MEM likely facilitates the oxidation of catechol by utilizing the generated H_2O_2 (Figure 2b). Peroxidase-mediated oxidation is a one-electron oxidation reaction that forms a semiquinone radical from catechol, unlike tyrosine- or periodate-mediated oxidation, which directly forms a quinone via two-electron oxidation. Thus, almost all the oxidized catechol might be consumed to form catechol adducts such as di-catechol for crosslinking rather than being oxidized further to quinone that can covalently bind to other nucleophilic functional groups such as the amine and thiol groups in ECM proteins.

To verify our hypothesis, the spectral change of the reaction solutions of HA-CA and HCM was examined using ultraviolet–visible (UV–vis) spectroscopy. In the UV–vis spectra of HA-CA, negligible variations were observed for up to 30 min after the initial reaction (Figure 2c). However, HCM 200 exhibited a significant increase in absorbance across a wide range of wavelengths from 280 to 400 nm (Figure 2c), which corresponds to oxidized catechol and catechol adducts such as di-catechol.[34,35] Interestingly, this phenomenon was not observed in the control group; the reaction solution of HA-CA with bovine serum albumin (HA-CA/BSA) was supplemented as a control protein (Figure 2c). This result indicates that the complex composition of biomolecules, including peroxidase in MEM, is likely to promote catechol oxidation.[7] It is noteworthy that the peak

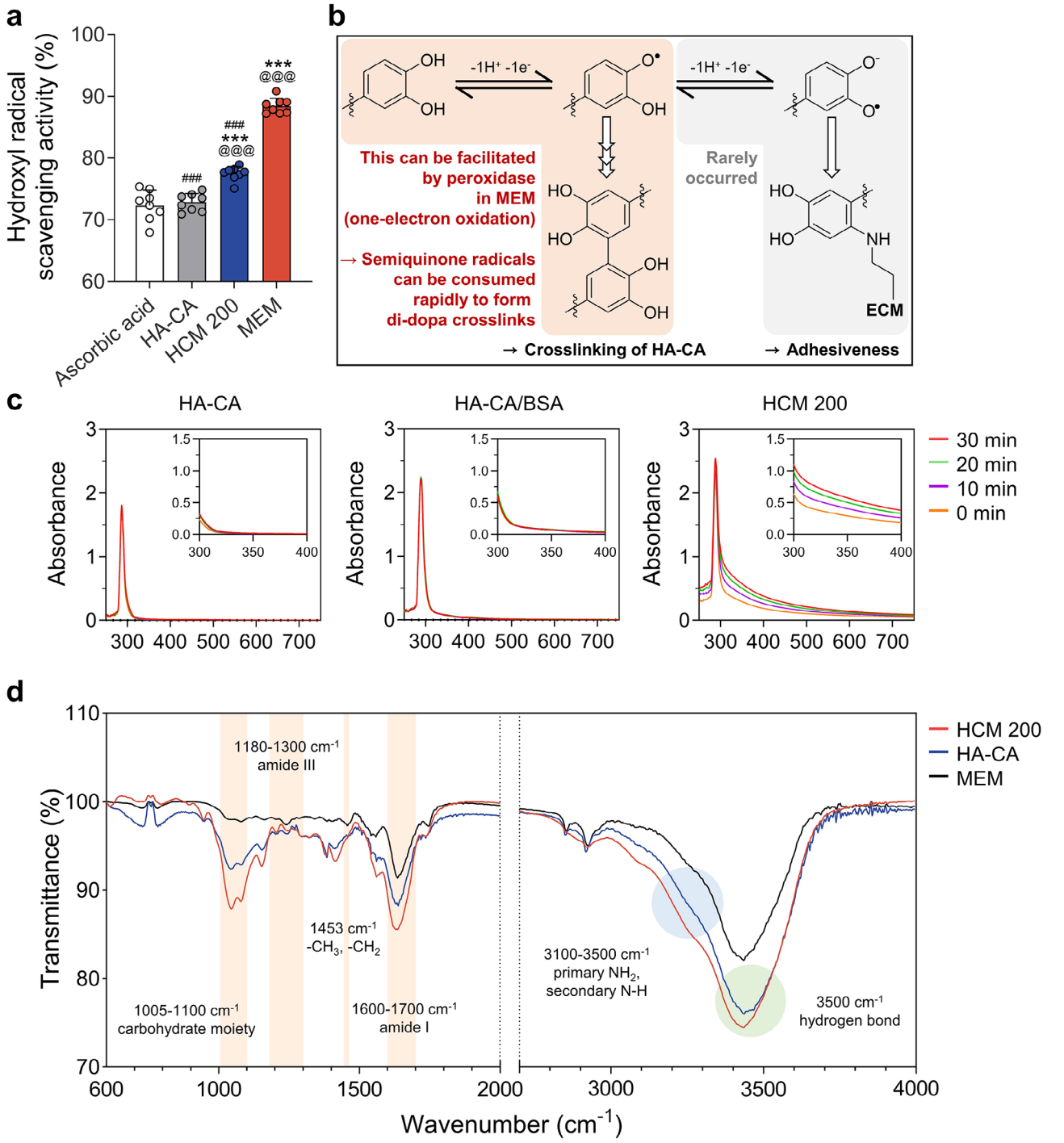

Figure 2. Evaluations of the crosslinking mechanism of HCM patch hydrogel. a) Hydroxyl radical scavenging activity of hydrogel with hydrogen peroxide ($n = 8$). b) A schematic flow of the proposed chemical mechanisms of HCM patch hydrogel. Spectroscopic analysis using c) UV–vis and d) FT-IR to examine the detailed chemical interactions between HA-CA and MEM. The statistical difference was determined with a one-way ANOVA. The results are shown as mean ± S.D. (***$p < 0.001$ vs HA-CA, $^{\#\#\#}p < 0.001$ vs MEM, and $^{@@@}p < 0.001$ vs ascorbic acid).

corresponding to the products of Michael addition between catechol and biomolecules (500–650 nm)[36] was relatively low (Figure 2c), which suggests that the covalent bonding between the catechol in HA-CA and biomolecules in MEM was not dominant. This result, in turn, indicates that the promotion of crosslinking in the HCM hydrogel did not rely significantly on covalent bonding through catechol oxidation during the crosslinking period.

In the Fourier transform infrared (FT-IR) spectrum of the HCM 200 hydrogel, the peaks corresponding to amide I and

amide III in the protein components shifted marginally compared with those for the MEM group (Figure 2d). This indicated the occurrence of interactions between HA-CA and MEM. Specifically, a shift was observed from 1635 to 1628 cm^{-1} for amide I and from 1238 to 1243 cm^{-1} for amide III (Figure 2d).[37,38] Additionally, the broad peak demonstrating hydrogen bonding in the HCM hydrogel shifted compared with that verified in the MEM group, indicating a major role of non-covalent networking (including hydrogen bonding) in the gelation of the HCM patch.[12] To summarize the UV–vis and FT-IR spectroscopy results, MEM can function as a crosslinking agent to promote oxidative crosslinking of catechol in HA-CA and participate in non-covalent interactions with catechol. Thereby, it effectively induces gelation of the HA-CA hydrogel through a balanced combination of covalent and non-covalent interactions.[12]

2.4. Proteomic Analysis of ECM in MEM

It was anticipated that MEM is crucial not only in the crosslinking of the hydrogel but also in providing a favorable biochemical microenvironment for tissue-specific regeneration. Therefore, a mass spectrometry-based proteomic analysis and an intensity-based absolute quantification (iBAQ)-based quantification were performed to investigate the protein composition of MEM in detail. The proteomic analysis revealed that MEM was predominantly composed of 85 matrisome proteins, which accounted for 65.7% of the total protein content. These included various types of collagens (18 proteins), glycoproteins (39 proteins), proteoglycans (10 proteins), ECM-affiliated proteins (10 proteins), and ECM regulators (8 proteins) (**Figure 3**a,b). The remaining 34.3% of the total amount of proteins in the MEM (275 proteins) were non-matrisome proteins. Among these, 255 proteins were identified as being expressed in skeletal muscle, and 24 proteins were recognized as skeletal muscle-enriched proteins, encoded by genes with more than a four-fold increase in mRNA expression levels in skeletal muscle compared to other tissues (Figure 3c left panel; Figure S4, Supporting Information). A mapping of the proteins identified in MEM based on their gene names and relative expression levels revealed that the top 61 proteins (accounting for 90% of the total protein content) included 27 matrisome proteins (Figure 3c, right panel). These matrisome proteins included collagen type VI (COL6A3, COL6A1, and COL6A2), collagen type I (COL1A1 and COL1A2), fibrillin (FBN1), fibrinogen (FGA), lumican (LUM), decorin (DCN), and fibromodulin (FMOD) (Figure 3c), which are known to be important for the movement and development of muscular tissue.[39–42] Collagen VI, which accounts for the highest content (35%, Figure 3c) in MEM, has been demonstrated to regulate satellite cell (SC) responses and induce muscle recovery.[43] Additionally, collagen I and lumican, each constituting ≈5% of the MEM content (Figure 3c), have been demonstrated to promote myogenesis. Herein, collagen I provide structural support, and lumican functions as an exerkine to enhance muscle regeneration processes.[42,44] These functional molecules in MEM have been demonstrated to promote myogenesis and muscle regeneration by supporting biochemical signaling and physical alignment, enhancing myogenic differentiation and maturation.[13,45]

A gene ontology (GO) analysis focusing on biological processes (BP) was performed to identify the functional roles of the MEM proteins. The GO-BP analysis revealed a substantial overlap in GO terms between proteins comprising 90% of the abundance and muscle-enriched proteins in MEM (e.g., muscle structure development, actin filament-based process, muscle contraction, and muscle system process) (Figure 3d,e; Figure S5, Supporting Information). These data indicate that proteins in the MEM may play a role in organizing the extracellular structure of muscle tissues and enhancing muscle functionality. Then, significant GO terms (p-values less than 0.05) were categorized and visualized using REViGO.[46] Among these, the three most significant GO terms were identified as "supramolecular fiber organization" (GO:0097435, $p = 4.43 \times 10^{-27}$), "muscle system process" (GO:0003012, $p = 3.65 \times 10^{-26}$), and "muscle structure development" (GO:0061061, $p = 9.78 \times 10^{-25}$). When the 316 statistically significant GO terms identified by the GO-BP analysis were grouped into super-clusters based on their correlation, the most representative super-clusters were "regulation of muscle contraction" (89 GO terms), "supramolecular fiber organization" (32 GO terms), and "muscle structure development" (27 GO terms) (Figure 3f). Further analysis of the non-matrisome protein relationship using Gorilla[47] highlighted a significant enrichment of GO terms such as "muscle filament sliding," "regulation of muscle contraction," and "muscle system process" (Figure S6, Supporting Information). These observations indicate that the MEM contains diverse tissue-specific molecules that provide a reparative biochemical microenvironment essential for muscle regeneration and maturation.

With regard to the tissue specificity of the tissue-derived matrix, we have previously reported the importance of tissue-specific ECM composition in creating biologically favorable environments for cellular processes. For example, gastrointestinal (GI) tissue-derived ECM hydrogels outperform non-GI ECM (e.g., muscle, skin, and lymph) hydrogels in supporting the viability and growth of GI organoids.[48] This enhanced bioactivity of the GI ECM is attributed to the higher abundance of critical GI tract-specific matrisome proteins compared to ECM from other tissue sources, especially those inducing epithelial cell–fibronectin assembly. Similarly, MEM is enriched in muscle-specific proteins and molecules related to the essential pathways for muscle development and regeneration, such as the PI3K/Akt and calcium signaling pathways.[49] These tissue-specific ECM components in the MEM contributed to better muscle tissue development in a muscle atrophy model than those in the skin ECM. Overall, we conclude that the tissue origin critically influences the bioactivities of the ECM and MEM, with muscle-specific molecular compositions promoting muscle regeneration.

2.5. Satellite Cell (SC) Activation by HCM Patch Hydrogel

The majority of SCs, also known as myogenic stem cells, are quiescent in muscle tissue and non-proliferative. However, these begin to migrate, proliferate, and differentiate into myoblasts in response to injury, and actively participate in muscle regeneration.[50] To apply the HCM patch hydrogel for cell-free therapeutic applications in muscle injury, we first evaluated

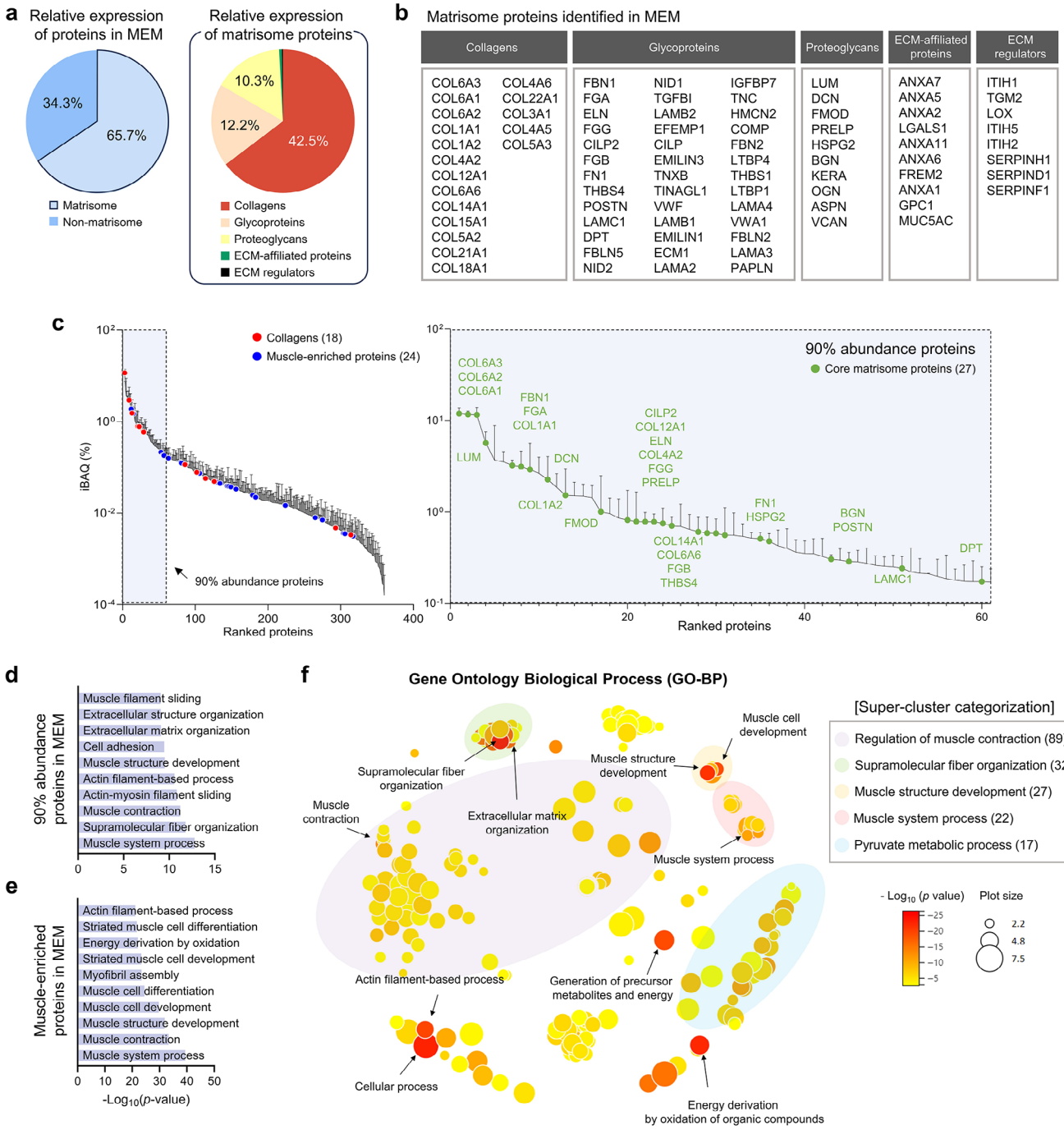

Figure 3. Proteomic characterization of MEM. a) Relative expression of matrisome, non-matrisome, and type of matrisome proteins in MEM. b) Matrisome proteins identified in MEM. c) The protein abundance encompasses 360 proteins, with collagens indicated by the red dots and muscle-enriched proteins by the blue dots. Core matrisome proteins (corresponding to collagen, glycoproteins, and proteoglycans), which were identified within the top 90% abundance range, are highlighted in green ($n = 3$). The top 10 enriched GO-BP terms of d) top 90% abundance proteins and e) muscle-enriched proteins in MEM. f) A semantic plot depicting the enriched GO-BP terms in the MEM proteins. The color of each small circle indicates the p-value, while its size reflects the occurrence of the GO terms, with larger circles representing terms that appear more frequently. Each GO term is classified into a super-cluster according to its relationship with the others. The terms represented in each super-cluster and the number of corresponding GO terms are indicated in the upper right box.

the biocompatibility of the hydrogel system using primary SCs. Live/dead staining revealed that most of the SCs incorporated in the HCM patch hydrogels (regardless of the amount of MEM in the construct) were alive during the 7 days of in vitro culture, demonstrating their favorable compatibility (Figure S7, Supporting Information).

Next, we evaluated the capability of the HCM patch hydrogel to induce SC activation and myogenic differentiation, which is a critical factor in muscle tissue reconstruction. Protein expression of myogenic markers was assessed by immunocytochemistry at days 3 and 7 of culture, allowing for evaluation of both early and late-stage myogenic markers. Immunocytochemistry revealed that the number of cells expressing paired box 7 (Pax7; a representative SC marker) increased significantly after 3 days in the HCM 200 patch hydrogel group (**Figure** 4a,c). Additionally, the number of Pax7 and desmin co-positive cells (corresponding to the activated SCs) was also the largest in the HCM 200 group (Figure 4a,c). Myogenin (MyoG) and myosin heavy chain (MF20) (a myogenesis marker and mature myogenic marker, respectively) were also enhanced in the HCM 200 group (Figure 4a,c). Quantitative real-time polymerase chain reaction (qPCR) analysis further demonstrated that the gene expression level of *Pax7* was enhanced significantly in the HCM 200 group, whereas that of myogenic factor 5 (*Myf5*; a myogenic progenitor marker) was similar in all the tested groups (Figure 4d). The expression of myoblast determination protein 1 (*MyoD*) and *MyoG* increased as the concentration of MEM increased, showing the highest levels in the HCM 200 group (Figure 4d).

On day 7 of culture, the number of Pax7 and desmin co-positive cells was not statistically different among the tested groups (Figure 4b,e). However, mature myogenic markers such as MyoG and MF20 were enhanced in the HCM patch hydrogel groups. Moreover, the SCs in the HCM 200 and 400 groups exhibited the highest expression levels (Figure 4b,e). In the qPCR analysis, there were no significant differences in early myogenic markers, including *Pax7* and *Myf5*, but the expression of *Pax7* in the HCM 200 group was the highest (Figure 4f). Similar to the results on day 3, the expression levels of *MyoD* in the HCM 100, 200, and 400 groups were over 1.5 times higher than those in the HA-CA_ox group (Figure 4f). The expression of *MyoG* was also upregulated in the HCM 50, 100, and 200 groups compared to the control group without MEM (HA-CA_ox) (Figure 4f). These observations indicate that the HCM patch hydrogel enhanced the SC proliferation and activation, with MEM playing a key role in promoting muscle tissue regeneration.

2.6. Biological Functionality of HCM Patch Hydrogel

The HCM 200 patch hydrogel demonstrated the long-term induction of SC activation and maturation. To further validate its biological functionality, we performed a migration assay to assess its capability to activate SCs at the injury sites. SCs densely seeded with a round-shaped mold were co-cultured with hydrogels using a transwell system, and spontaneous cellular activation and movement were initiated by removing the fixed mold (Figure 4g). After 7 days of culture, a significantly enhanced SC migration was observed in the HCM group, while the oxidatively cross-linked HA-CA hydrogel (with $NaIO_4$) did not show any improvement in SC migration compared with the non-treated group (NT) (Figure 4g,h). These results indicate that the biochemical molecules of MEM from the HCM patch hydrogel might induce the activation of SCs.

In general, proteins or various substrates can be anchored tightly within catechol-modified hydrogel systems because of the strong covalent interactions between the molecules and catechols.[12,30,50] Although oxidative covalent interactions occur in HCM patch hydrogels, we anticipated that loosely incorporated MEM via non-covalent interactions could be released from the hydrogel and function as a biochemical cue for enhanced tissue regeneration. To verify our hypothesis, the HCM patch hydrogel crosslinked by oxidation using $NaIO_4$ was used as a control (HCM_ox) that contained more covalent bonds than the HCM hydrogel crosslinked spontaneously by MEM. After 1 day of incubation in PBS, an initial burst release of MEM was observed in both groups (Figure 4i). However, when covalent interactions were dominant during hydrogel crosslinking (HCM_ox; HA-CA patch hydrogel with MEM crosslinked by a conventional method using $NaIO_4$ oxidant), there was no additional release of MEM from the hydrogel, whereas MEM-crosslinked HCM (HCM 200) showed a sustained release profile of MEM until day 80 (Figure 4i). During the period for investigating SC activation and migration by MEM released from the HCM 200 hydrogel (≈45% MEM release up to 1 week in Figure 4i) (Figure 4b,g), the size of the HCM patch did not significantly change after the initial swelling. Taken together, MEM supports the biocompatible gelation of HA-CA hydrogels and provides a sustained release mechanism, contributing to SC activation and subsequent muscle tissue regeneration. Therefore, we selected the HCM 200 patch hydrogel for the subsequent in vivo experiments.

2.7. Application of HCM Patch Hydrogel in the VML Mouse Model

The in vivo applicability of the HCM patch hydrogel was assessed to evaluate its stability and ability to form a hydrogel structure without the need for additional oxidants. The HA-CA and HCM 200 patches were implanted into the subcutaneous tissue and left to spontaneously form hydrogel structures without the addition of oxidants. A day after implantation, the HCM 200 patch formed a stable hydrogel and adhered to the implantation site, whereas a significant portion of the HA-CA patch was not detected by the macroscopic and histological examination, and only adipose tissue of the subcutaneous fascia area was observed (Figure S8, white space, Supporting Information). A histological analysis based on H&E and toluidine blue (TB) staining revealed no excessive inflammation or observable fibrotic response around the HCM hydrogels during 7 days of implantation. A further investigation of the tissues using MT staining on day 7 revealed minimal fibrotic tissue formation, indicating excellent in vivo compatibility of the HCM patch hydrogel (Figure S9, Supporting Information). The stability of the HCM patch hydrogel in vivo was evaluated by measuring its swelling ratio following subcutaneous implantation. The HCM 200 patch hydrogel maintained a stable hydrogel structure at the implantation site for 7 days (Figure S10, Supporting Information).

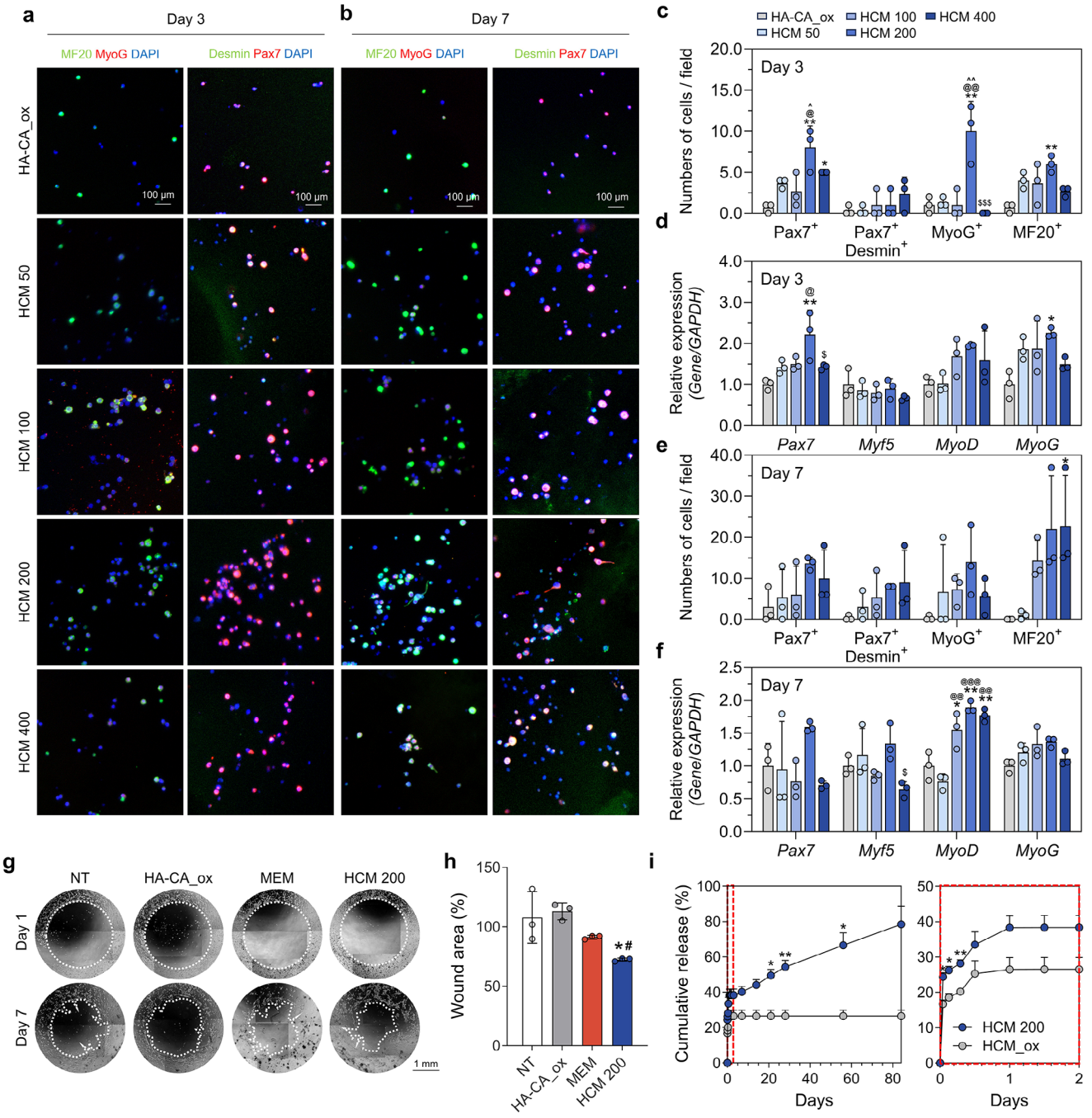

Figure 4. Evaluation of HCM patch hydrogel in satellite cell (SC) activation. Fluorescence images showing immunostaining of Pax7, Desmin, MyoG, and MF20 on a) day 3 and b) day 7 of the culture of SCs in each hydrogel. Quantification of each marker in the fluorescence images ($n = 3$) on c) day 3 and e) day 7 of the culture. qPCR analysis for comparing gene expressions of SC and myoblast markers on d) day 3 and f) day 7 of the culture ($n = 3$). g) Migration assay to inspect the biological function of the HCM patch hydrogel in activating SCs and h) quantitative analysis of the covered area after the SC migration ($n = 3$). The wound area is indicated with a white dotted line. The HA-CA_ox group indicates the HA-CA patch treated with $NaIO_4$ oxidant. i) Cumulative amount of the MEM proteins released from the hydrogels (HCM and HCM_ox; HA-CA patch hydrogel with MEM crosslinked by a conventional method using $NaIO_4$ oxidant, $n = 5$). The statistical difference was determined with a one-way or two-way ANOVA. The results are shown as mean ± S.D. ($^{\#}p < 0.05$ vs NT; $^{*}p < 0.05$ and $^{**}p < 0.01$ vs HA-CA_ox; $^{@}p < 0.05$, $^{@@}p < 0.01$, and $^{@@@}p < 0.001$ vs HCM 50; $^{\hat{}}p < 0.05$ and $^{\hat{}\hat{}}p < 0.01$ vs HCM 100; and $^{\$}p < 0.05$ and $^{\$\$\$}p < 0.001$ vs HCM 200).

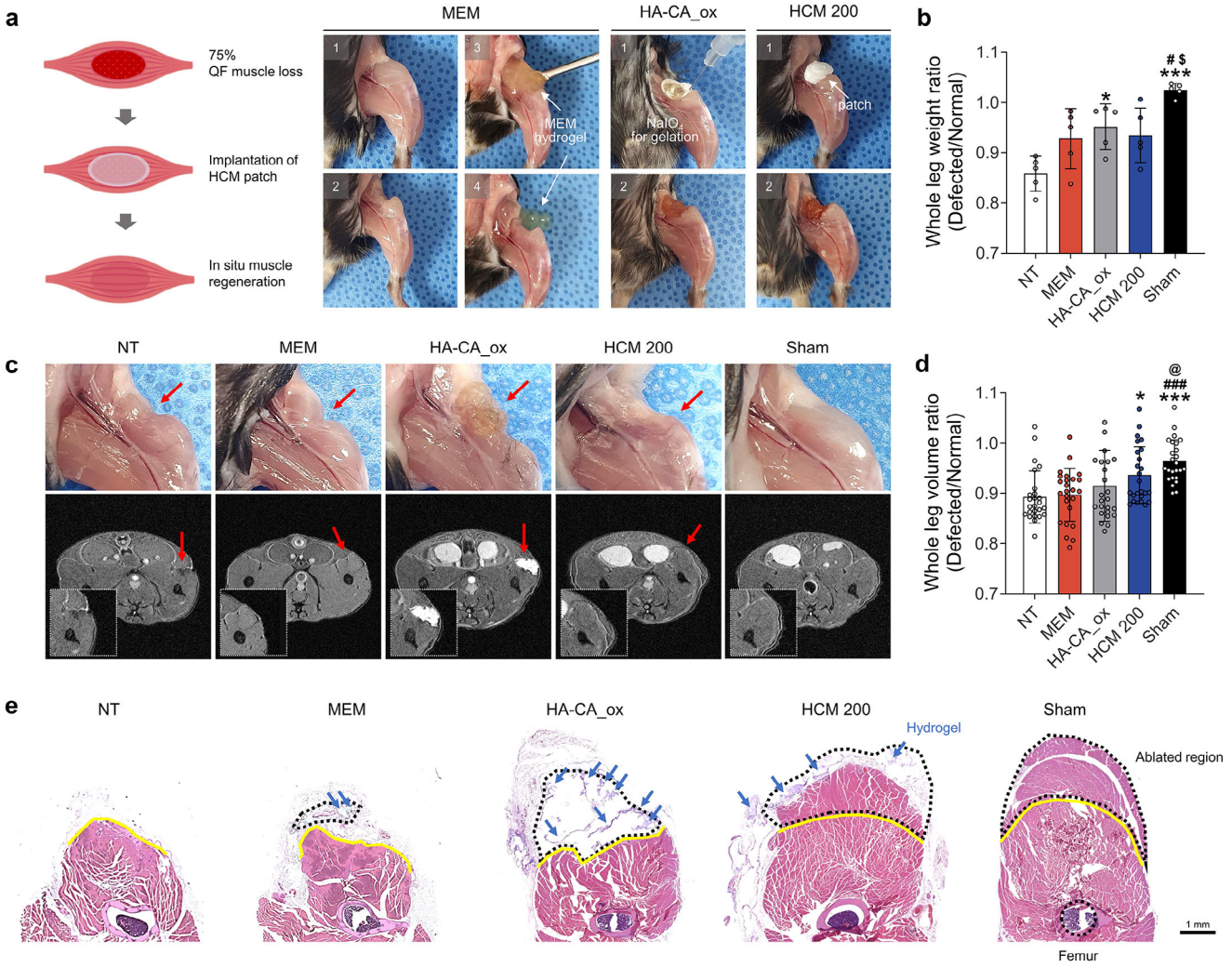

Figure 5. Implantation of HCM patch hydrogel in a mouse model of volumetric muscle loss (VML). a) Schematic illustration of HCM patch hydrogel-mediated muscle repair following VML. Surgical procedure for implanting constructs. A series of photographs illustrates the implantation of the construct to the ablated site. The MEM hydrogel and HCM 200 patch hydrogel were placed on the injury site. In the case of the HA-CA patch hydrogel crosslinked by oxidant (HA-CA_ox), it was necessary to add an oxidizing agent ($NaIO_4$) for gelation. Once gelation was complete, the patch was rinsed with PBS. b) At week 12, the weight ratio comparison was made between the defective and contralateral normal legs ($n = 5$; the data are expressed as mean ± SEM). The HA-CA_ox group indicates the HA-CA patch treated with $NaIO_4$ oxidant. c) Magnetic resonance T2 imaging to track the implanted constructs 12 weeks after implantation. The red arrows indicate the defect region, the dark areas represent defects that were not filled, the white areas correspond to materials with high water content, and the gray areas represent well-integrated muscle tissue. d) The volume ratio of the defective leg to the contralateral normal legs at week 12 ($n = 25$; the data are expressed as mean ± S.D.). The statistical difference was determined by a one-way ANOVA ($^{*}p < 0.05$ and $^{***}p < 0.001$ vs NT, $^{\#}p < 0.05$ and $^{\#\#\#}p < 0.001$ vs MEM, $^{@}p < 0.05$ vs HA-CA_ox, and $^{\$}p < 0.05$ vs HCM 200). e) Histological analysis of muscle tissues with the implanted patch hydrogel constructs in volumetric muscle loss (VML) mouse model. H&E-stained images of the injured quadriceps skeletal muscle compartment at week 12. The ablated region corresponds to ≈90% loss of the fascia latae and 60% of the rectus femoris. This results in a volumetric reduction of ≈75% in the quadriceps skeletal muscle compartment. Yellow lines indicate the margin of the original injury, and black-dashed lines outline the implanted hydrogel constructs remaining within the ablated region or the expected region of the ablation in the Sham group (scale bar = 1 mm).

To assess the capability of the HCM patch hydrogel in muscle tissue regeneration, HA-CA_ox, MEM, and HCM 200 were implanted into a mouse model of VML with 75% removal of the quadriceps femoris muscle (**Figure 5a**). MEM and HA-CA_ox were selected as the control groups to isolate and reflect the contributions of each component to SC activation and muscle regeneration. At 12 weeks post-implantation, the entire leg was retrieved, and the tissue mass was measured. The weight ratio of defective to normal muscles revealed muscle mass recovery in all the treated groups, but there was no significant difference between the types of materials (Figure 5b). Meanwhile, T2-weighted magnetic resonance imaging (MRI) of the quadriceps femoris muscle revealed a significant improvement in regeneration in the HCM 200 group (Figure 5c,d). Compared with the Sham group, the cavity of the defect was not recovered in the NT and MEM groups, whereas the tissue mass was restored sufficiently

in HCM 200 (Figure 5c). Although HA-CA_ox also filled the cavity, a substantial portion of the tissue exhibited an abnormal water content (depicted as a white area), indicating that rather than the tissue mass being restored, the HA-CA polymer remained in the hydrogel state.[51] As a result, the muscle volume ratio of defective to normal muscles calculated using T2-weighted MRI was found to be significantly improved only in the HCM 200 group (Figure 5d). The disparity in Figure 5b,d may have resulted from the variations in the physical properties of the HA-CA_ox and HCM 200 hydrogels. Interestingly, the HCM 200 hydrogels remained in place through 12 weeks of implantation (Figure 5c), demonstrating a degradation rate lower than that observed in the in vitro experiment (Figure 1i). From these results, we conclude that the HCM 200 hydrogels degrade gradually in an in vivo environment and are suitable for supporting the gradual development of new muscle mass, providing a durable framework and gradual release of MEM molecules to facilitate tissue regeneration over time. In contrast, the HA-CA patch hydrogel crosslinked with $NaIO_4$ (HA-CA_ox) exhibited better mechanical properties and a longer degradation profile,[14] which may have hindered the integration of the regenerated muscle with the surrounding tissue.[52] Thus, significant tissue reconstruction was achieved only in the HCM 200 group.

2.8. Enhanced Muscle Regeneration and Locomotive Function by HCM Patch Hydrogel in the VML Model

The regenerative potential of HCM patch hydrogel was further evaluated through histological examinations. At 12 weeks post-implantation, H&E staining at a lower magnification revealed a substantial recovery of the damaged tissue in the HCM 200 group, while the other groups exhibited significantly lower tissue restoration (Figure 5e). Higher-magnification images of MT staining and fibrosis quantification (**Figure 6**a,d) revealed minimal fibrosis in the HCM 200 group, indicating effective muscle regeneration with minimal scarring. In contrast, the NT group exhibited extensive fibrosis with irregular, disorganized collagen and myofibers containing centralized nuclei (Figure 6a,c,d).[53] Fibrotic collagen is typically more disorganized and denser, while the naturally occurring collagen in healthy muscle tissue is more structured and aligned.[54] The HCM 200 group displayed predominantly mature myofibers throughout the newly formed tissues. Meanwhile, the MEM and HA-CA_ox groups showed a mixed structure of mature and centrally nucleated myofibers in conjunction with fibrotic tissues (Figure 6a,c,d). Additionally, immunostaining for myosin heavy chain 1E (MyH1E), which plays a crucial role in muscle contraction and development, showed a significant enhancement in myofiber maturation with proper laminin deposition in the HCM 200 group, compared with the NT, MEM, and HA-CA_ox groups (Figure 6b). To evaluate the morphological and structural development of the regenerated muscle, we measured the minimal Feret's diameter and cross-sectional area (CSA) of the newly formed myofibers, which serve as indicators of dystrophic and normal muscle phenotypes. Notably, only the HCM 200 group displayed CSA and minimal Feret's diameter frequency distributions comparable to those of the Sham group, whereas the MEM and HA-CA_ox groups exhibited distributions resembling those of the NT group (Figure 6e; Figure S11, Supporting Information).

Given the significant improvement in muscle regeneration observed in the HCM 200 group, we hypothesized that the observed outcomes may be attributed to an enhanced SC activation by HCM 200. While SC activation and differentiation typically occur within a week, the sustained release of MEM from the HCM 200 hydrogel over 80 days (Figure 4i) may contribute to prolonged SC activation and migration, supporting muscle regeneration over an extended period. To validate this hypothesis, we conducted immunofluorescence staining for PAX7 and MyoD in muscle tissue sections from an in vivo experiment 12 weeks after transplantation (Figure S12, Supporting Information). The results revealed that Pax7-positive and MyoD-negative quiescent SCs increased across the treated groups (MEM, HA-CA_ox, and HCM 200 groups; Figure S12a,b, Supporting Information). Importantly, the largest number of Pax7 and MyoD double-positive activated SCs was observed in the HCM 200 group (Figure S12a,c, Supporting Information), supporting that HCM 200 increased the overall SC population and contributed to their activation and accelerated muscle regeneration. These findings align with previous studies demonstrating that tissue scaffolds and bioactive molecules can support the maintenance of their long-term activity.[55,56]

Enhanced vascularization is another important indicator of improved tissue regeneration, as it plays a crucial role in applying essential nutrients to injured tissues, thereby promoting structural and functional restoration.[57] When the retrieved tissues were stained with markers related to the vascularization, a considerably large number of α-smooth muscle actin (α-SMA)-positive vessels and CD31-positive capillaries were observed in the HCM 200 group, compared with the other control groups (Figure 6f–h). We performed additional immunofluorescence staining against CD31 and α-SMA to assess the number of mature blood vessels, which is crucial for successful muscle regeneration. It is noteworthy that only the HCM 200 group exhibited a statistically significant increase in the number of CD31 and α-SMA double-positive vessels (arterioles) compared with the NT group (Figure S13, Supporting Information). This demonstrated the more mature vascularization in the HCM 200 patch hydrogel-treated group.

Finally, we examined the functional restoration of VML mice using a Rotarod test over 11 weeks post-treatment. As a result, HCM 200 enhanced motor coordination and improved the functional recovery in the impaired limb, indicated by the exceptional endurance on a rotating rod, both at constant and accelerating speeds, in comparison to the NT group (Figure 6i; Figure S14, Supporting Information). With regard to the therapeutic efficacy of the HCM 200 hydrogels, a significant enhancement in motor coordination was observed. Moreover, the functional improvement over time, in conjunction with histological analysis and behavioral assessments, demonstrated the most significant therapeutic potential of the HCM hydrogels in terms of new tissue formation and functional recovery. The superior therapeutic effects of HCM compared with those of MEM and HA-CA_ox can be attributed to its unique combination of mechanical and biological properties, which provide structural stability and promote muscle regeneration. Compared with MEM, the HCM hydrogel provides a biochemical environment conducive to cellular activity and demonstrates significantly better mechanical properties

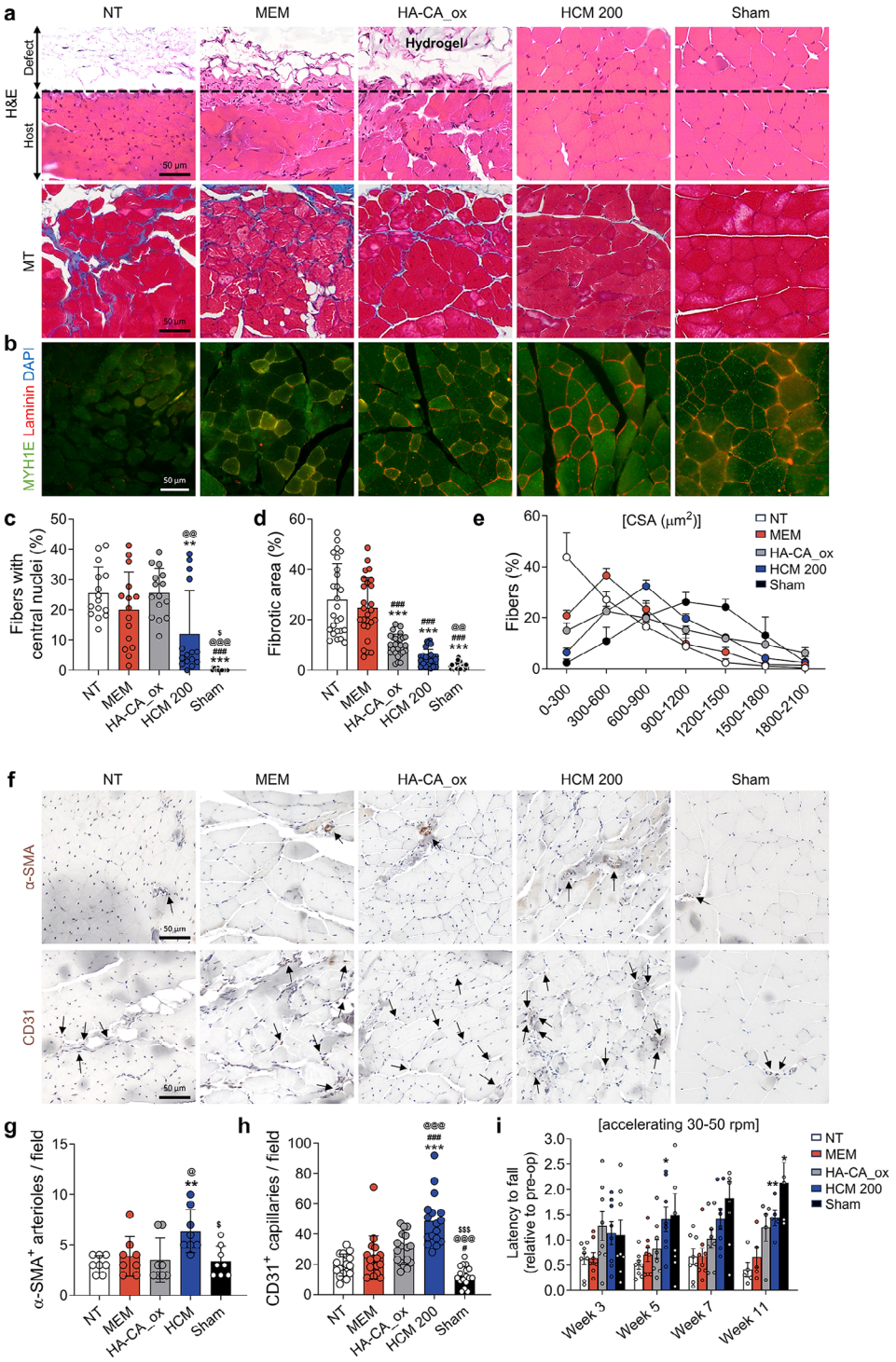

Figure 6. Evaluation of HCM patch hydrogel in muscle tissue regeneration in VML mouse model at 12 weeks. a) H&E and Masson's trichrome (MT) stained images of the newly formed muscle area in the defective region. The HA-CA_ox group indicates the HA-CA patch treated with $NaIO_4$ oxidant. b) Immunohistochemical staining against laminin and myosin heavy chain 1E (MYH1E). c) Quantification of centrally nucleated fibers ($n = 15$), d) fibrotic area ($n = 26$), and e) distribution of the cross-sectional area (CSA) of myofibers in the *de novo* formed tissue region ($n = 3$; the results are displayed as mean ± SEM, and the statistical processing results are shown in Figure S11, Supporting Information). f) Immunohistochemical staining against α-SMA and CD31. g) Measurement of the number of α-SMA-positive vessels ($n = 8$) and h) CD31-positive capillaries per field ($n = 17$). i) Rotarod tests under acceleration from 30 to 50 rpm at 3, 5, 7, and 11 weeks after hydrogel implantation. The sample size was $n = 8$ for weeks 3, 5, and 7, and $n = 5$ for week 11. The data are expressed as mean ± SEM. All data, unless stated otherwise, are presented as mean ± S.D. The statistical difference was determined with a one-way or two-way ANOVA ($^{*}p < 0.05$, $^{**}p < 0.01$, and $^{***}p < 0.001$ vs NT; $^{\#}p < 0.05$ and $^{\#\#\#}p < 0.001$ vs MEM, $^{@}p < 0.05$, $^{@@}p < 0.01$, and $^{@@@}p < 0.001$ vs HA-CA_ox; and $^{\$}p < 0.05$ and $^{\$\$\$}p < 0.001$ vs HCM 200).

and tissue adhesiveness (Figure 1d,e,g). These enhanced material properties enable a more stable mechanical and biological support, thereby facilitating effective tissue growth at the defect site. In contrast, HA-CA_ox is devoid of MEM-mediated biological function, while it showed a stable tissue adhesion with mechanical support. Although the mechanical properties of the materials used are important for tissue regeneration, previous studies have emphasized that the ECM provides structural integrity and actively regulates cell behavior through its biochemical and biophysical properties, which in turn influence cellular fate and tissue organization.[58,59] Considering the harsh conditions in the animal model used in this study, additional validation is required to further demonstrate the therapeutic efficacy of HCM hydrogels in restoring locomotive function. These validations could involve muscle defect models with less severe damage (30–50% muscle loss), which would allow for a more detailed observation of muscle regeneration and recovery and enable a better comparison of the therapeutic efficacy of the treatment developed in our study.[60,61]

3. Conclusion

In this study, we introduced a strategy for treating muscular injury by developing a composite HCM patch hydrogel that integrates biocompatible adhesive polymers with muscle tissue-derived ECM. Our results highlight the significant advantages of the HCM patch hydrogel, primarily its capability to be crosslinked via both covalent and non-covalent interactions without relying on conventional oxidants. This eliminates the drawbacks associated with oxidant-based cross-linking methods, thereby providing a safer, more efficient, and potentially more clinically viable alternative. Moreover, the HCM patch hydrogel demonstrated a remarkable capacity to stimulate satellite cells, which in turn ultimately enhanced muscle tissue regeneration. Although the modulus of our material did not directly match that of the native muscle, the HCM patch hydrogel provided mechanical and biochemical cues that were particularly favorable for creating a regenerative microenvironment. This strategy represents a significant advancement in the field of in situ muscle regeneration and provides a potential cell-free therapeutic solution for muscular injuries.

4. Experimental Section

Preparation of MEM: To prepare MEM, porcine triceps brachii muscle purchased from a local butcher shop was decellularized according to a previously reported protocol.[24] The muscle was sliced into small pieces and washed with triple-distilled water (tDW) to remove contaminants and blood. The muscle tissue pieces were agitated in 1% (v/v) sodium dodecyl sulfate (SDS; Wako, Osaka, Japan) for 48 h and then in 1% (v/v) Triton X-100 (Wako) with 0.1% ammonium hydroxide (Sigma–Aldrich, St. Louis, MI, USA) for 2 h for decellularization. The decellularized tissues were agitated in tDW to completely remove the detergent and sterilized in 1% (v/v) penicillin/streptomycin (Thermo Fisher Scientific, Waltham, MA, USA) for 2 h. Finally, the tissues were rinsed one more time in tDW, freeze-dried, and stored at −20 °C until use. The agitations during the decellularization process were performed at 4 °C and 180 rpm. The lyophilized MEM was solubilized using a protein digest solution of 4 mg mL^{-1} pepsin (Sigma–Aldrich) in 0.02 M hydrochloride (Sigma–Aldrich) at room temperature. Following the protocol applied in a previous study,[24] the MEM hydrogel was prepared by mixing solubilized MEM with PBS and tDW and neutralizing with sodium hydroxide (Sigma–Aldrich) to attain a final concentration of 5 mg mL^{-1}. The mixture was incubated at 37 °C for 30 min to facilitate gelation.

Characterization of MEM: To verify the removal of cellular components by decellularization, the DNA in the muscle tissues before and after decellularization was isolated using a DNA extraction kit (Bioneer, Daejeon, Korea). The DNA concentrations were quantified with Quant-iT PicoGreen dsDNA Assay Kits (Thermo Fisher Scientific). To evaluate the preservation of the ECM components, the glycosaminoglycan (GAG) content in the muscle tissues before and after decellularization was quantified using 1,9-dimethyl methylene blue dye (Sigma–Aldrich) solution according to a previously reported procedure.[62,63]

Proteomic Analysis of MEM: For the proteomic analysis of MEM, proteins were extracted using a Filter-Aided Sample Preparation (FASP) kit (Abcam, Cambridge, UK) according to the manufacturer's protocol. The extracted proteins were analyzed using liquid chromatography-tandem mass spectrometry (LC-MS/MS) according to the method described in a previous study.[13] The resulting mass spectrometry data were processed using MaxQuant software (version 1.6.17.0) for protein identification and an evaluation of the protein composition and abundance. The identified proteins were categorized based on the ECM Atlas database.[49] GraphPad Prism 9.0 (GraphPad Software, San Diego, CA, USA) was used to visualize the ECM protein identification, categorization, composition, and abundance. To identify significantly enriched biological processes, a GO enrichment analysis was conducted using the PANTHER overrepresentation test, with *Sus scrofa* selected as the reference species in the GO Ontology database.[64] The GO enrichment analysis results were further refined and visualized using REViGO.[46] Meanwhile, the relationships among non-matrisome proteins were examined and visualized using Gorilla.[47] GraphPad Prism (version 9.0) was employed to generate additional GO analysis-related visualizations, including plots and summaries.

Synthesis of HA-CA: The HA-CA polymer was synthesized via carbodiimide chemistry according to previously reported procedures.[14] HA (molecular weight [MW] 200 kDa, Lifecore Biomedical, Chaska, MN, USA) was dissolved fully in tDW to a concentration of 1% (w/v). Next, 1-(3-dimethylaminopropyl)-3-ethylcarbodiimide hydrochloride (EDC, Thermo Fisher Scientific) was added to the HA solution at an HA to EDC molar ratio of 1:3. The solution was permitted to react for 10 min at pH 5.5. N-hydroxysuccinimide (NHS, Sigma–Aldrich) was incorporated into the reaction solution at an HA to NHS molar ratio of 1:3, and the solution was stirred for 20 min at pH 5.5–6.0. After activating the carboxyl groups in HA using EDC/NHS, dopamine hydrochloride (Sigma–Aldrich) was added to the solution at an HA to dopamine molar ratio of 1:3. The reaction solution was permitted to react for 24 h at pH 4.5–5.0. The unreacted molecules and by-products were removed by dialysis using a semi-permeable membrane (Cellu/Sep T2 dialysis membrane with a MW cutoff of 6–8 kDa; Membrane Filtration Products Inc., Seguin, TX, USA) in acidic PBS (Biosesang, Seongnam, Korea) and tDW. The resultant solution was lyophilized and stored at −20 °C before use.

Preparation and Characterization of Patch Hydrogel: To prepare HA-CA patches, the lyophilized HA-CA polymer was dissolved in PBS (Sigma–Aldrich) at a concentration of 1% (w/v). The HA-CA solution was poured into a predesigned mold and then lyophilized. The HA-CA patch hydrogel was created by applying 5 µL of $NaIO_4$ solution (4.5 mg mL^{-1}, Sigma–Aldrich) per 2 mg of HA-CA patch to induce oxidative crosslinking of the HA-CA polymer. Similarly, the HCM patch was prepared by dissolving the HA-CA polymer at a concentration of 1% (w/v) together with MEM powder at a predetermined concentration (50, 100, 200, and 400 µg mL^{-1}) and freeze–drying the mixture solution. MEM powder was prepared by treating MEM with pepsin digest solution at a concentration of 20 mg mL^{-1} for 48 h, followed by freeze–drying. The HCM patch hydrogel was formed via self-crosslinking by applying 5 µL of PBS per 2 mg of HCM patch for in vitro experiments or by simply applying the HCM patch to the desired site for in vivo experiments.

The internal structure of the patch hydrogels was examined with images captured using field-emission SEM (FE-SEM, 7001F, JEOL, Tokyo, Japan). The samples for SEM analysis were prepared by dehydrating the

hydrogels by immersing them in serial dilutions of ethanol and t-butyl alcohol (Sigma–Aldrich) for 30 min (in each solution). The hydrogels were frozen in t-butyl alcohol and lyophilized for imaging. The freeze-dried samples were then sectioned using a blade to expose the internal structure, and SEM images were acquired from five different regions of the scaffold to qualitatively assess the distribution of MEM. The internal pore size of the patch hydrogel was measured using ImageJ software (National Institute of Health, Bethesda, MD, USA) based on the SEM images.

Spectroscopic Analysis of Crosslinking Mechanisms: For the UV–vis spectroscopy analysis, UV–vis spectra of the 1% (w/v) HA-CA solution and the HA-CA solution mixed with MEM solution (200 μg mL^{-1}) (HCM 200) or BSA solution (200 μg mL^{-1}) (HA-CA/BSA) were analyzed using a V-650 UV–vis spectrophotometer (JASCO Corporation, Tokyo, Japan) at predetermined time points (0, 10, 20, and 30 min). Lyophilized MEM hydrogels, HA-CA patches, and HCM 200 patches were prepared for FT-IR spectroscopy analysis. The transmittance profiles were obtained using an FT-IR spectrometer (Vertex 70, Bruker, Billerica, MA, USA) as reported previously.[65]

Primary Mouse Satellite Cell Isolation: The animal experimental procedures were approved by the Institutional Animal Care and Use Committee (IACUC) of Yonsei University (permit number: IACUC-A-201901-862-03). SCs were isolated from the thigh and lower leg muscle tissues of C57BL/6J mice (6-week-old males, 18–20 g, Orientbio, Seongnam, Korea) as described previously.[66] The isolated SCs were cultured on 0.1 mg mL^{-1} collagen type 1 (Corning, NY, USA)-coated plates in an SC proliferation medium composed of F-10 Medium (Thermo Fisher Scientific) containing a basic fibroblast growth factor (R&D Systems, Minneapolis, MN, USA), 1% (v/v) GlutaMAX (Thermo Fisher Scientific), 20% (v/v) horse serum (Thermo Fisher Scientific), and 1% (v/v) penicillin and streptomycin (P/S, Thermo Fisher Scientific). For myogenic differentiation, the proliferation medium was replaced with a myogenic induction medium composed of Dulbecco's Modified Eagle's medium (Thermo Fisher Scientific) containing 1% (v/v) GlutaMax, 2% (v/v) horse serum, and 1% (v/v) P/S.

In Vitro Biocompatibility: To evaluate the cytotoxicity of the patch hydrogels, SCs were applied at a density of 2×10^2 cells per square millimeter of the patch area. The viability of the cells was visualized using a live/dead viability and cytotoxicity assay kit (Thermo Fisher Scientific) according to the manufacturer's instructions and quantified by calculating the proportion of live cells to the total cells counted (live cells + dead cells). The live/dead assay was performed at three-time points (days 0, 3, and 7) after seeding the SCs onto the patch hydrogel.

Cell Migration Test: To evaluate the SC activation, a cell migration assay was conducted according to previously reported procedures with marginal modifications.[67] Briefly, 2.5 mm diameter polydimethylsiloxane (Dow Corning, Auburn, MI, USA) stoppers were fixed firmly into a 24-well plate, and 2.5×10^5 SCs per well were seeded on the plates. After 24 h of cell adhesion, the stoppers were removed, and the cells were permitted to migrate spontaneously into the defect. Cells were co-cultured with hydrogels using a transwell system and cultured in a myogenic induction medium, which was replaced every 2 days. The NT group refers to a group that did not receive any treatment. After 7 days of incubation, the migration area of the cells into the exclusive region was assessed using ImageJ software (National Institutes of Health, Bethesda, MD, USA).

Satellite Cell Activation by Patch Hydrogel: SCs were seeded onto the HCM patch hydrogel at a density of 2×10^4 cells mm^{-2} of the patch area. In the in vitro experiment for SC activation, the SCs were cultured in a myogenic induction medium immediately after seeding onto the patch hydrogels, and the medium was maintained for the entire observation period. qPCR or immunocytochemistry analysis was conducted at 3 and 7 days post-cell seeding to evaluate the activation and differentiation of SCs.

Applications of Hydrogels in Animal Models with Muscle Defects: Ethical approval for the animal experimental procedures was obtained from the IACUC of Yonsei University (permit number: IACUC-A-201901-862-03) and Yonsei University Health System (permit number: 2020-0035). The animals were provided with food and water in alternating 12 h light/dark cycles and maintained in a temperature-controlled animal care facility following animal protection regulations. The mice used in the experiments weighed between 18 and 20 g. To prepare the VML model, C57BL/6J mice (6-week-old males, Orientbio, Seongnam, Korea) were anesthetized with a mixture of ketamine (100 mg kg^{-1}, Yuhan, Seoul, Korea) and xylazine (10 mg kg^{-1}, Bayer Korea, Ansan, Korea). Then, 75% of the quadratus femoris muscle was removed, as reported previously.[13] Then, mice were assigned randomly to each group and treated using the prepared constructs: 5 mg mL^{-1} MEM hydrogel (MEM), HA-CA patch hydrogel crosslinked with oxidant (HA-CA_ox), and HCM patch hydrogel containing 200 μg mL^{-1} of MEM (HCM 200). The NT group refers to a group that did not receive any treatment. After the surgical ablation of the muscular tissues, the patch constructs were placed over the defect to fill the cavity of the removed tissue with the treated materials, anticipating replacement with newly regenerated tissues. The size of the implanted constructs was adjusted to align with the dimensions of the defect site, considering their swelling properties. This ensured effective coverage and integration with the injured area. For the HA-CA_ox hydrogel, gelation was achieved in situ by adding an oxidizing agent (4.5 mg mL^{-1} $NaIO_4$), followed by washing with PBS to remove the residual oxidizing agent thoroughly. In the Sham group, the outer skin at the defect site was incised and closed by suturing following the surgical procedure for the other groups.

Anatomical images were acquired by a T2-weighted fast spin-echo MRI sequence (9.4T MRI; Bruker, Billerica, MA, USA). Magnetic resonance spectroscopy was performed on a $1 \times 1 \times 1$ mm voxel using a point-resolved spectroscopy sequence without water suppression. The functional performance of the mice was assessed in constant (40 rpm) and acceleration (30–50 rpm) paradigms using a Rota-Rod (57601; Stoelting Co., Wood Dale, IL, USA) 1 week before surgery and 3, 5, 7, and 11 weeks after surgery. The time required to fall off the rod was recorded two times during each test, which lasted for up to 300 s. After the experiment, the weight ratio of the entire leg (from the femoral head area to the removed outer skin) was determined by measuring the entire leg of each mouse. Five mice were used for this analysis. The weight of the regenerated tissue at the defect site was normalized to that of the contralateral uninjured leg, resulting in a sample size of five, with one measurement per mouse. In contrast, the quadriceps skeletal muscle volume ratio was calculated using magnetic resonance T2 imaging. For each mouse, five slides with a thickness of 1 mm were captured from the defect site covering the entire affected region. The volume ratio was determined by integrating the volume measurements from all five slides for each mouse and normalizing these to the volume of the corresponding contralateral uninjured leg. Because five slides were analyzed for each of the five mice, this method yielded a total sample size of 25. These distinct approaches account for the differences in sample sizes between the weight and volume measurements.

Histological and Immunohistochemical Examination: The porcine muscle tissue after decellularization and the mouse muscle tissue from the 12-week VML model were preserved in 10% formalin (Sigma–Aldrich) and paraffin-embedded for sectioning. For the histological analysis, 4–6 μm sections were deparaffinized and stained with hematoxylin (Sigma–Aldrich), Eosin Y (Samchun Chemical, Seoul, Korea) (H&E), MT, and TB (Sigma–Aldrich). The muscle fibers with centrally located nuclei in the stained samples were counted using the multipoint tool in ImageJ. The fibrosis in the damaged regions was quantified using the blue-colored collagen content based on MT (Sigma–Aldrich) staining and analyzed using ImageJ software. Representative images for H&E staining were selected from the margins of the injury, whereas the muscle tissue adjacent to the injury margins was stained and analyzed for MT staining.

For immunohistochemical staining, the sections were deparaffinized and subjected to heat-induced antigen retrieval. The sections were then permeabilized with Triton X-100 (Sigma–Aldrich). The nonspecific binding was blocked with a mixture of horse serum (Thermo Fisher Scientific) and bovine serum albumin (MP Biomedicals LLC, Santa Ana, CA, USA). The sections were maintained overnight at 4 °C with the following primary antibodies MyH1E (Developmental Studies Hybridoma Bank, Iowa, IA, USA), laminin (LM; Sigma–Aldrich), α-SMA (Santa Cruz Biotechnology, Dallas, TX, USA), and CD31 (Abcam). All primary antibodies utilized in the analysis were specifically tailored to target mouse-derived proteins. This selective design ensures that any signals detected in the data correspond solely to mouse-specific substances, thereby distinguishing them from potential

porcine-derived components in the MEM. Following incubation, the sections were treated with PBS and subsequently with the secondary antibodies Alexa Fluor 488 goat anti-mouse immunoglobulin G (IgG) (Thermo Fisher Scientific) and Alexa Fluor 594 goat anti-rabbit IgG (Thermo Fisher Scientific). Sections of tissue incubated with primary antibodies were detected using the VECTASTAIN Elite ABC HRP system and DAB HRP substrate (Vector Laboratories, Burlingame, CA, USA). The sections were subsequently counterstained with 4′,6-diamidino-2-phenylindole (DAPI; TCI America, Portland, OR, USA) or hematoxylin for the cell nuclei. The stained slides were observed under a laser scanning confocal microscope (LSM 880; Zeiss, Jena, Germany) or VS120-S5-W slide scanner (Olympus, Tokyo, Japan). The cross-sectional size and minimum Feret diameter of the myofibers were determined using the area and circumference tools framed manually in ImageJ.[24] Additionally, the vessel formation within the newly regenerated muscles was quantified by assessing the number of α-SMA-positive microvessels and CD31-positive capillaries in the tissue sections. Representative images for the immunohistochemical analysis were selected from the muscle tissue adjacent to the injury margins.

Statistical Analysis: The data are presented as mean ± standard deviation (SD) or mean ± standard error of the mean (SEM), as specified in the figure legends. The statistical analyses were performed using the appropriate methods for each experiment. To compare the two groups, a two-tailed Student's t-test was used, whereas one- or two-way analysis of variance (ANOVA) followed by Tukey's post-hoc test (where necessary) was used for multiple group comparisons. A significance level of 0.05 was set for all the tests. The assumptions of homogeneity of variance were verified using Brown–Forsythe and Bartlett's tests depending on the data distribution. The statistical analyses were performed using GraphPad Prism 9 (GraphPad Software, San Diego, CA, USA).

Supporting Information

Supporting Information is available from the Wiley Online Library or from the author.

Acknowledgements

This work was supported by the National Research Foundation of Korea (NRF) grants (RS-2021-NR059722 and 2022R1C1C1011682) funded by the Korean government and the Ministry of Science and ICT (MSIT); Technology Innovation Program (20024298, Materials/Components Technology Development Program) funded by the Ministry of Trade, Industry & Energy (MOTIE, Korea); Yonsei Signature Research Cluster Program of 2025-22-0015; the Yonsei Fellow Program funded by Lee Youn Jae; and Cellartgen, Inc.; and Korean Fund for Regenerative Medicine grant funded by the Korean government (MSIT, the Ministry of Health & Welfare) (23B0103L1).

Conflict of Interest

S.-W. C. is the chief technology officer (CTO) of Cellartgen, Inc., Republic of Korea.

Data Availability Statement

The data supporting the observations of this study are available from the corresponding author upon request.

Keywords

adhesive hydrogel, decellularized matrix, muscle regeneration, patch hydrogel, volumetric muscle injury

Received: September 29, 2024
Revised: March 31, 2025
Published online: April 24, 2025

[1] S. Gardner, M. Frecklington, K. Rose, M. R. Carroll, *Prosthet. Orthot. Int.* **2024**, *48*, 368.
[2] M. Samandari, J. Quint, A. Rodríguez-delaRosa, I. Sinha, O. Pourquié, A. Tamayol, *Adv. Mater.* **2022**, *34*, 2105883.
[3] S. Testa, E. Fornetti, C. Fuoco, C. Sanchez-Riera, F. Rizzo, M. Ciccotti, S. Cannata, T. Sciarra, C. Gargioli, *Biomedicines* **2021**, *9*, 564.
[4] J. A. Larouche, E. C. Wallace, B. D. Spence, E. Buras, C. A. Aguilar, *JCI Insight* **2023**, *8*, 162835.
[5] S. Kiran, P. Dwivedi, V. Kumar, R. L. Price, U. P. Singh, *Cells* **2021**, *10*, 2016.
[6] C. Zhang, B. Wu, Y. Zhou, F. Zhou, W. Liu, Z. Wang, *Chem. Soc. Rev.* **2020**, *49*, 3605.
[7] S. An, E. J. Jeon, S. Y. Han, J. Jeon, M. J. Lee, S. Kim, M. Shin, S.-W. Cho, *Small* **2022**, *18*, 2202729.
[8] P. K. Forooshani, B. P. Lee, *J. Polym. Sci. A Polym. Chem.* **2017**, *55*, 9.
[9] N. Pandey, L. Soto-Garcia, S. Yaman, A. Kuriakose, A. U. Rivera, V. Jones, J. Liao, P. Zimmern, K. T. Nguyen, Y. Hong, *Biomater. Adv.* **2022**, *134*, 112589.
[10] C. Xie, X. Wang, H. He, Y. Ding, X. Lu, *Adv. Funct. Mater.* **2020**, *30*, 1909954.
[11] Y. Li, J. Cheng, P. Delparastan, H. Wang, S. J. Sigg, K. G. DeFrates, Y. Cao, P. B. Messersmith, *Nat. Commun.* **2020**, *11*, 3895.
[12] W. Zhang, R. Wang, Z. Sun, X. Zhu, Q. Zhao, T. Zhang, A. Cholewinski, F. K. Yang, B. Zhao, R. Pinnaratip, P. K. Forooshani, B. P. Lee, *Chem. Soc. Rev.* **2020**, *49*, 433.
[13] Y. Jin, E. J. Jeon, S. Jeong, S. Min, Y. S. Choi, S. H. Kim, J. S. Lee, J. Shin, J. H. Yu, D.-H. Ahn, Y.-G. Kim, H. S. Yang, T. J. Kang, S.-R. Cho, N. Choi, S.-W. Cho, *Adv. Funct. Mater.* **2021**, *31*, 2006227.
[14] J. Shin, S. Choi, J. H. Kim, J. H. Cho, Y. Jin, S. Kim, S. Min, S. K. Kim, D. Choi, S.-W. Cho, *Adv. Funct. Mater.* **2019**, *29*, 1903863.
[15] B. Kang, J. Shin, H.-J. Park, C. Rhyou, D. Kang, S.-J. Lee, Y.-S. Yoon, S.-W. Cho, H. Lee, *Nat. Commun.* **2018**, *9*, 5402.
[16] P. M. Costa, D. A. Learmonth, D. B. Gomes, M. P. Cautela, A. C. Oliveira, R. Andrade, J. Espregueira-Mendes, T. R. Veloso, C. B. Cunha, R. A. Sousa, *Polym. J.* **2021**, *13*, 3317.
[17] C. Guyot, T. Malaret, F. Touani Kameni, M. Cerruti, S. Lerouge, *ACS Appl. Bio Mater.* **2023**, *6*, 2875.
[18] X. Zhang, X. Chen, H. Hong, R. Hu, J. Liu, C. Liu, *Bioact. Mater.* **2022**, *10*, 15.
[19] C. R. Lee, Y. J. Lee, B. Y. Kwon, S. J. Lee, Y. H. Ryu, J.-W. Rhie, S.-H. Moon, *Tissue Eng. Regen. Med.* **2023**, *20*, 59.
[20] M. M. Smoak, K. J. Hogan, K. J. Grande-Allen, A. G. Mikos, *Sci. Adv.* **2021**, *7*, abg4123.
[21] P. Duran, F. Boscolo Sesillo, M. Cook, L. Burnett, S. A. Menefee, E. Do, S. French, G. Zazueta-Damian, M. Dzieciatkowska, A. J. Saviola, M. M. Shah, C. Sanvictores, K. G. Osborn, K. C. Hansen, M. Shtrahman, K. L. Christman, M. Alperin, *Sci. Transl. Med.* **2023**, *15*, abj3138.
[22] E. Lih, K. W. Park, S. Y. Chun, H. Kim, T. G. Kwon, Y. K. Joung, D. K. Han, *ACS Appl. Mater. Interfaces* **2016**, *8*, 21145.
[23] J. Jia, E. J. Jeon, M. Li, D. J. Richards, S. Lee, Y. Jung, R. W. Barrs, R. Coyle, X. Li, J. C. Chou, M. J. Yost, S. Gerecht, S.-W. Cho, Y. Mei, *Sci. Adv.* **2020**, *6*, aaz5894.
[24] Y. Jin, D. Shahriari, E. J. Jeon, S. Park, Y. S. Choi, J. Back, H. Lee, P. Anikeeva, S.-W. Cho, *Adv. Mater.* **2021**, *33*, 2007946.
[25] J. Shin, J. H. Cho, Y. Jin, K. Yang, J. S. Lee, H. J. Park, H. S. Han, J. Lee, H. Jeon, H. Shin, S.-W. Cho, *Small* **2016**, *12*, 6266.
[26] S. Choi, E. J. Jeon, Y. Bae, J. Jeon, D. Kang, H. Lee, S.-W. Cho, *Appl. Mater. Today* **2024**, *39*, 102318.
[27] H. Yuk, J. Wu, T. L. Sarrafian, X. Mao, C. E. Varela, E. T. Roche, L. G. Griffiths, C. S. Nabzdyk, X. Zhao, *Nat. Biomed. Eng.* **2021**, *5*, 1131.
[28] S. J. Wu, J. Wu, S. J. Kaser, H. Roh, R. D. Shiferaw, H. Yuk, X. Zhao, *Nat. Commun.* **2024**, *15*, 1215.
[29] M. R. Natowicz, Y. Wang, *Clin. Chim. Acta.* **1996**, *245*, 1.

[30] W. Y. Quan, Z. Hu, H. Z. Liu, Q. Q. Ouyang, D. Y. Zhang, S. D. Li, P. W. Li, Z.-M. Yang, *Molecules* **2019**, *24*, 2586.
[31] E. Kim, M. Kang, H. Liu, C. Cao, C. Liu, W. E. Bentley, X. Qu, G. F. Payne, *Front. Chem.* **2019**, *7*, 541.
[32] M. H. Mannino, R. S. Patel, A. M. Eccardt, R. A. Perez Magnelli, C. L. C. Robinson, B. E. Janowiak, D. E. Warren, J. S. Fisher, *Comp. Biochem. Physiol. B Biochem. Mol. Biol.* **2019**, *234*, 9.
[33] R. Pinnataip, B. P. Lee, *ACS Omega* **2021**, *6*, 5113.
[34] S. Hong, Y. Wang, S. Y. Park, H. Lee, *Sci. Adv.* **2018**, *4*, aat7457.
[35] P. Velander, L. Wu, S. B. Hildreth, N. J. Vogelaar, B. Mukhopadhyay, R. F. Helm, S. Zhang, B. Xu, *Pharmacol. Res.* **2022**, *184*, 106409.
[36] E. Fuentes-Lemus, P. Hägglund, C. López-Alarcón, M. J. Davies, *Mol.* **2021**, *27*, 15.
[37] S. H. Hendawy, H. F. Alzan, H. S. Abdel-Ghany, C. E. Suarez, G. Kamel, *Sci. Rep.* **2024**, *14*, 8515.
[38] Y. Ji, X. Yang, Z. Ji, L. Zhu, N. Ma, D. Chen, X. Jia, J. Tang, Y. Cao, *ACS Omega* **2020**, *5*, 8572.
[39] J. M. Grasman, M. J. Zayas, R. L. Page, G. D. Pins, *Acta Biomater.* **2015**, *25*, 2.
[40] W. Zhang, Y. Liu, H. Zhang, *Cell Biosci.* **2021**, *11*, 65.
[41] K. Asano, A. Cantalupo, L. Sedes, F. Ramirez, *Int. J. Mol. Sci.* **2022**, *23*, 1892.
[42] H. J. Cho, Y.-S. Lee, D. A. Kim, S. A. Moon, S. E. Lee, S. H. Lee, J.-M. Koh, E. Lumican, *Int. J. Mol. Sci.* **2022**, *23*, 10031.
[43] A. Urciuolo, M. Quarta, V. Morbidoni, F. Gattazzo, S. Molon, P. Grumati, F. Montemurro, F. S. Tedesco, B. Blaauw, G. Cossu, G. Vozzi, T. A. Rando, P. Bonaldo, *Nat. Commun.* **2013**, *4*, 1964.
[44] D. Wang, F. Chang, Z. Guo, M. Chen, T. Feng, M. Zhang, X. Cui, Y. Jiang, J. Li, Y. Li, J. Yan, *Tissue Cell* **2024**, *90*, 102506.
[45] S. An, E. J. Jeon, M. Kim, S. Y. Han, Y. S. Song, J. Jeon, J.-U. Park, S. W. Cho, *Chem. Eng. J.* **2024**, *485*, 149906.
[46] F. Supek, M. Bošnjak, N. Škunca, T. Šmuc, *PLoS One* **2011**, *6*, 21800.
[47] E. Eden, R. Navon, I. Steinfeld, D. Lipson, Z. Yakhini, *BMC Bioinformat.* **2009**, *10*, 48.
[48] S. Kim, S. Min, Y. S. Choi, S. H. Jo, J. H. Jung, K. Han, J. Kim, S. An, Y. W. Ji, Y.-G. Kim, S.-W. Cho, *Nat. Commun.* **2022**, *13*, 1692.
[49] S. Choi, M. J. Lee, M. Kim, Y. Bae, J. U. Park, S. W. Cho, *Adv. Healthcare Mater.* **2024**, *13*, 2401826.
[50] D. I. Shin, Y. J. Jin, S. Noh, H.-W. Yun, D. Y. Park, B.-H. Min, *Tissue Eng. Regen. Med.* **2024**, *21*, 487.
[51] Y. C. Dong, M. Bouche, S. Uman, J. A. Burdick, D. P. Cormode, *ACS Biomater. Sci. Eng.* **2021**, *7*, 4027.
[52] T. Chen, Z. Cai, X. Zhao, G. Wei, H. Wang, T. Bo, Y. Zhou, W. Cui, Y. Lu, *J. Nanobiotechnol.* **2024**, *22*, 289.
[53] Y. Yoshimoto, M. Ikemoto-Uezumi, K. Hitachi, S. I. Fukada, A. Uezumi, *Front. Cell Dev. Biol.* **2020**, *8*, 267.
[54] D. Van De Vlekkert, E. Machado, A. d'Azzo, *Bio Protoc* **2020**, *10*, 3629.
[55] T. H. Qazi, D. J. Mooney, M. Pumberger, S. Geissler, G. N. Duda, *Biomaterials* **2015**, *53*, 502.
[56] P. Sousa-Victor, L. García-Prat, P. Muñoz-Cánoves, *Nat. Rev. Mol. Cell Biol.* **2022**, *23*, 204.
[57] D. Gholobova, L. Terrie, M. Gerard, H. Declercq, L. Thorrez, *Biomaterials* **2020**, *235*, 119708.
[58] A. Mishra, U. Modi, R. Sharma, D. Bhatia, R. Solanki, *Biomed. Eng. Adv.* **2025**, *9*, 100143.
[59] J. M. Muncie, V. M. Weaver, *Curr. Top. Dev. Biol.* **2018**, *130*, 1.
[60] E. E. Vega-Soto, B. L. Rodriguez, R. E. Armstrong, L. M. Larkin, *Regen. Eng. Transl. Med.* **2020**, *6*, 62.
[61] B. M. Sicari, V. Agrawal, B. F. Siu, C. J. Medberry, C. L. Dearth, N. J. Turner, S. F. Badylak, *Tissue Eng., Part A* **2012**, *18*, 1941.
[62] J. S. Lee, Y. S. Choi, J. S. Lee, E. J. Jeon, S. An, M. S. Lee, H. S. Yang, S.-W. Cho, *Chem. Eng. J.* **2022**, *427*, 130926.
[63] J.-W. Seo, S.-H. Jo, S.-H. Kim, B.-H. Choi, H. Cho, J. J. Yoo, S.-H. Park, *Tissue Eng. Regen. Med.* **2024**, *21*, 209.
[64] H. Mi, A. Muruganujan, X. Huang, D. Ebert, C. Mills, X. Guo, P. D. Thomas, *Nat. Protoc.* **2019**, *14*, 703.
[65] J. H. Cho, J. S. Lee, J. Shin, E. J. Jeon, S. An, Y. S. Choi, S.-W. Cho, *Adv. Funct. Mater.* **2018**, *28*, 1705244.
[66] B. Gharaibeh, A. Lu, J. Tebbets, B. Zheng, J. Feduska, M. Crisan, B. Péault, J. Cummins, J. Huard, *Nat. Protoc.* **2008**, *3*, 1501.
[67] J. Kim, J. Kim, H.-J. Park, E. J. Jeon, S.-W. Cho, *Korean J. Chem. Eng.* **2023**, *40*, 903.